(Received 4 September 2025, Accepted 17 November 2025, Scheduled 22 December 2025)

Beam Steering, Biodegradable MIMO DRA: A 3D-Printed Solution for Wideband and High-Isolation C-Band Applications

Bingi Naresh Kumar*, Metuku Shyam Sunder, and Dasari Ramakrishna

ECE Department, University College of Engineering, Osmania University, Hyderabad, India

ABSTRACT: In this study, we describe a compact two-port MIMO dielectric resonator antenna (DRA) system made from biodegradable polylactic acid (PLA) using additive manufacturing techniques. Performance goals were achieved through a systematic performance study on the pin height, pin position, cavity width, and cavity length. The simulated results showed a wide range of bandwidth from 5.0 to 7.4 GHz with return loss ($|S_{11}|$) lower than -10 dB corresponding to a fractional bandwidth of approximately 36.8%. Excellent port isolation is achieved with $|S_{21}| < -20$ dB consistent across the entire band. The antenna provides more than 10 dBi gain with a high directivity making it useful for high-performance wireless applications. Furthermore, diversity MIMO performance confirms exceptional diversity performance with the Envelope correlation coefficient (ECC) remaining below 0.015 and ideal Diversity Gain (DG) of 10 dB. Another important feature is the electronic beam steering capability of this antenna, enabled by adjusting the phase difference between the two ports. With excitation phase shifts of 0°, 90°, 180°, and 270°, the antenna's main beam can be steered between broadside and unidirectional directions, providing flexible spatial coverage through dynamic phase control, rather than switching among fundamentally different radiation patterns. The employment of environmentally friendly PLA materials paired with 3D printing technology fosters sustainable practices for antenna development while simultaneously permitting inexpensive prototype creation and swift adaptability in the design changes. This MIMO DRA system can be extensively employed in C-band applications like the 5G communication systems, satellite downlink services, radar systems, and high-speed wireless data links, where it is crucial to have wide bandwidth, high isolation, and compact size.

1. INTRODUCTION

The exponential growth of wireless communication technologies has triggered an increasing demand for compact, high-performance antennas capable of supporting the stringent requirements of modern systems such as 5G networks, Wi-Fi 6E/7, radar, and satellite communications [1–3]. These technologies require antennas that offer wide operational bandwidths, high gain, directional radiation, low mutual coupling, and reliable diversity performance, especially in Multiple-Input Multiple-Output (MIMO) configurations [4–6]. Among various antenna technologies, Dielectric Resonator Antennas (DRAs) have emerged as a compelling solution in the microwave frequency range owing to their low conduction losses, high radiation efficiency, design flexibility, and compatibility with planar feeding structures [7].

C-band (4–8 GHz) has become increasingly vital due to its favourable balance between propagation characteristics and available bandwidth and is widely used in mid-band 5G communication systems, satellite downlink services, air traffic control radar, and military surveillance [8]. For these applications, antenna systems must be engineered to operate efficiently within this band while maintaining compact dimensions and minimizing interference between ports in MIMO scenarios [6, 7]. The main design challenges are achieving broadband impedance matching, high isolation, and low envelope correlation in a limited physical footprint [9, 10].

Recent years have seen a parallel push toward sustainable engineering practices, driven by environmental concerns and the global shift toward eco-friendly materials and manufacturing. This has motivated researchers to explore biodegradable materials such as Polylactic Acid (PLA), a thermoplastic derived from renewable biomass sources, for Dielectric Resonator Antenna [11–13]. PLA materials are biodegradable, have relatively low environmental impact, and are easily processed through additive manufacturing (3D printing), facilitating customizability and reducing both prototyping cost and turnaround time [13, 14]. Additive manufacturing enables the fabrication of complex geometries with high precision, making it ideal for dielectric structures like DRAs, while overcoming the expense and brittleness of traditional ceramics [11, 14]. Although PLA features a lower dielectric constant and higher loss tangent, proper design optimization and geometric tuning can yield performance suitable for targeted wireless applications [12–14].

One of the most important features of MIMO antenna systems is that the mutual coupling between elements should be low, which, in turn, provides uncorrelated signal paths that have a significant impact on system throughput and error resilience [5, 6, 9, 10]. Parameters such as the Envelope Correlation Coefficient (ECC) and Diversity Gain (DG) are some of the main criteria, where ECC values significantly lower than 0.5 and DG values close to 10 dB are considered as indicators of excellent diversity performance. Besides that, phase-dependent beam steering allows a further spatial coverage extension, as the main radiation lobe direction can be changed dynamically

* Corresponding author: Bingi Naresh Kumar (b.nareshy12@gmail.com).

without any mechanical movement. Here the antenna performs beam steering through the electronic change of port excitation phases, which is just a particular and feasible way of radiation pattern reconfigurability for the directional control [15, 16].

In this study, we propose a 2-port MIMO DRA system fabricated using PLA via 3D printing, operating efficiently in the C-band. A comprehensive multi-stage optimization includes systematic tuning of metallic pin height, pin position, cavity width, and cavity length, to enhance impedance bandwidth, isolation, and overall radiation performance. The optimized antenna achieves a wide impedance bandwidth from 5.0 GHz to 7.4 GHz, $|S_{11}|$ below -10 dB, and inter-port isolation ($|S_{21}|$) consistently better than -20 dB. The design demonstrates peak gain above 10 dBi, excellent directivity, low ECC (< 0.015), and DG approaching 10 dB, confirming its suitability for MIMO applications.

The outcomes validate the potential of eco-friendly materials in high-frequency antenna design and demonstrate the effectiveness of additive manufacturing for rapid prototyping of compact, high-performance MIMO systems for next-generation wireless technologies. This approach presents a promising path toward sustainable, scalable, and high-performance solutions for 5G mid-band, satellite communications, and C-band radar applications.

2. ANTENNA DESIGN AND CONFIGURATION

Dielectric Resonator Antenna (DRA) is designed such that the corners of the rectangular DRA are aligned along the $\pm X$ and $\pm Y$ axes, which are rotated by 45 degrees with respect to the corners of the ground plane and substrate as illustrated in Fig. 1 and Fig. 2. Also, DRA is integrated with a substrate which has length = width = 50 mm (S_L) and height (S_H) = 2 mm, to eliminate the losses due to the inaccuracy of positioning or displacement of the DR; therefore, the proposed antenna is fabricated in a single piece. The dielectric in the proposed system as rectangular dielectric resonator antenna (RDRA) and substrate is Poly Lactic Acid (PLA), which has a dielectric constant (ε_r) of 3.45 and dielectric loss tangent (δ) = 0.035.

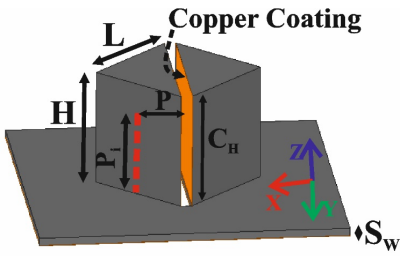

FIGURE 1. Isometric view.

The DRA has equal length (L), width (W), and height (H), each measuring 30 mm. The proposed MIMO antenna system is excited from the bottom, i.e., from the ground plane side which has length = width = 50 mm and height = 0.035 mm, using a coaxial feeding mechanism with a characteristic impedance of 50 ohms. The radius of coaxial probe is $P_r = 0.6$ mm.

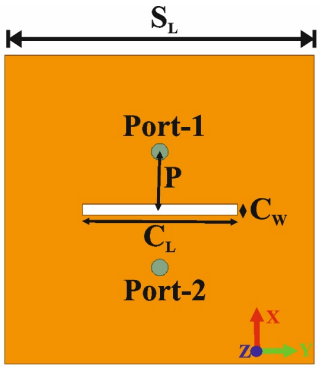

FIGURE 2. Bottom view.

Both ports are optimized for better impedance matching as well as isolation, and both ports are placed at the position (P) from the center of the antenna system. Pins of both ports are inserted into the RDRA in an effort of attaining the broad bandwidth of $|S_{11}| \leq -10$ dB, and the inserted pin's height (P_i) is 22.5 mm. Further, the isolation within both ports is enhanced by introducing a diagonal cavity along Y-axis, having length (C_L) = 40 mm, width (C_W) = 3 mm, and height (C_H) = 30 mm, i.e., C_H extends through the full height of the DRA, substrate, and ground, thereby forming a hollow structure at the center of the antenna system. The walls facing each other are masked with a copper tape with a height $M_H = C_H$, which is connected with the ground plane.

The permittivity of the proposed antenna is altered with the cavity slots cut in the RDRA, and it will become an effective permittivity (ε_{eff}) of the DR with a smaller value. Thus, as the ε_{eff} decreases, the Q factor decreases, which also helps the bandwidth enhancement. Hence, ε_{eff} of the proposed DRA can be calculated by modifying the dielectric waveguide model.

3. DESIGNING METHODOLOGY AND PARAMETRIC STUDY

This research aims extensively at the improvement of the impedance bandwidth of a 3D-printed 2-port MIMO RDRA, as well as the demonstration of electronic beam steering through phase-controlled port excitation, which is the steering method that would allow for efficient and adaptive C-band coverage. The steering method of this design is achieved through setting varying excitation phases at the two ports and then driving accordingly.

The design process for the MIMO RDRA, based on the proposed idea, involved a series of deliberate, sequential steps, which are detailed in Fig. 3 with a flow chart. First off, the reference structure was a rectangular DRA, and it was investigated. To achieve impedance matching and a wider bandwidth, the height of the probe feed was optimized. After that, the probe position was changed to improve the field coupling and resonance merging. So, to confine fields, enhance isolation, and stabilize gain performance, a metal cavity was finally introduced. The impact of each iteration of the design on $|S_{11}|$, $|S_{21}|$, and gain was reviewed to lead the refinement. The transition stages exhibited noteworthy enhancements in bandwidth (from 17.5%

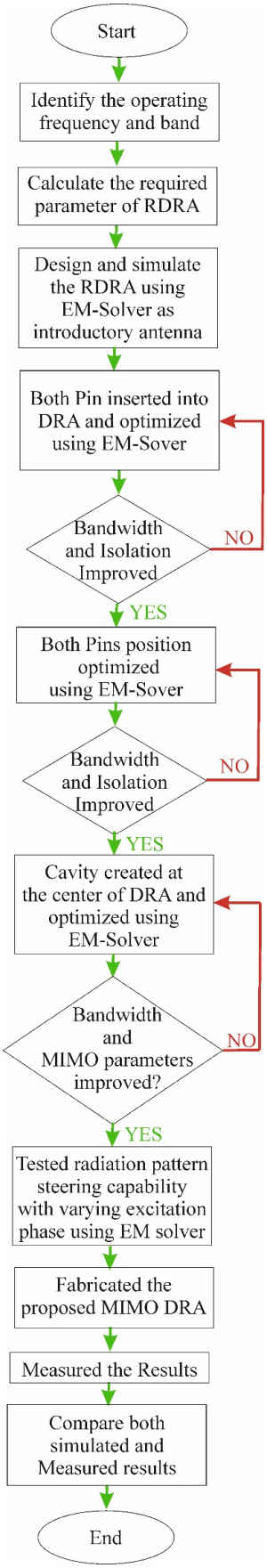

FIGURE 3. Design evolution flowchart of the proposed MIMO RDRA.

to 36.8%) and isolation (from 10 dB to > 20 dB) of the last refined configuration.

4. EFFECT OF HEIGHT OF PINS

Initially, a ground plane and substrate having length = width = 80 mm (S) and $S_H = 2$ mm is adopted. At the same time, a Rectangular Dielectric Resonator (RDR) is placed at the centre of the substrate having $L = W = 30$ mm and $H = 30$ mm. The theoretical formula for resonant frequency (f_r) of an RDRA is given as:

$$f_r = \frac{c}{2\pi\sqrt{\varepsilon_r}}\sqrt{k_x^2 + k_y^2 + k_z^2} \tag{1}$$

where "ε_r" is the dielectric constant of the RDRA; "c" is the speed of light in free space; and symbols "k_x", "k_y", and "k_z" represent the wavenumbers in the x, y, and z directions, respectively.

Fig. 4(a) shows the curves of the reflection coefficient ($|S_{11}|$ in dB) with frequency for different values of pin insertion heights (P_i) in a Dielectric Resonator Antenna (DRA), where P_i ranges from 20 mm to 25 mm. It can be observed that $|S_{11}|$ curve is the deepest when $P_i = 23$ mm (approximately -14 dB), and its resonance is centred around 5.7 GHz, lower than the target frequency of 6 GHz, which is the centre frequency of the C-band of the microwave spectrum. In contrast, $P_i = 22.5$ mm provides a slightly higher $|S_{11}|$ (around -12.5 dB), but its resonant frequency is centred much closer to 6 GHz. Since this is the first step in the optimization process, selecting $P_i = 22.5$ mm allows us to start with a configuration already near the target frequency.

In MIMO systems, $|S_{21}|$ indicates the mutual coupling between the two antenna ports — lower values (typically below -20 dB) reflect better isolation, which is essential for minimiz-

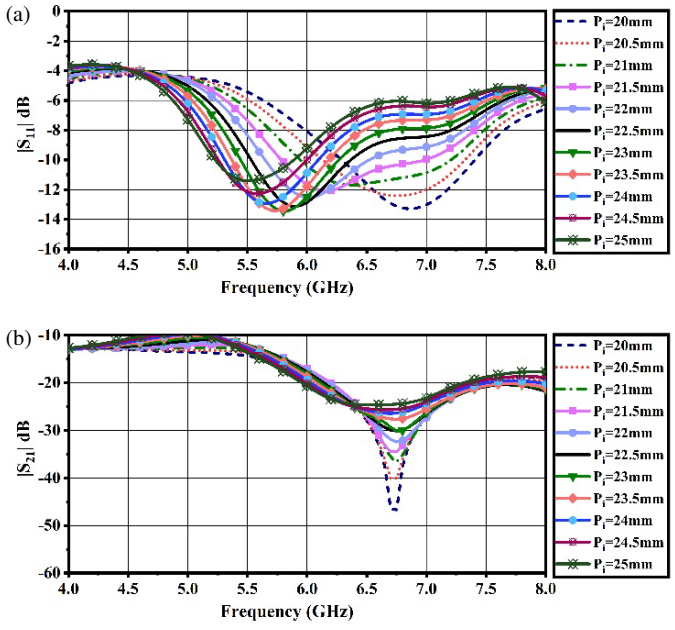

FIGURE 4. S parameter variation for different value of P_i. (a) Reflection coefficient. (b) Isolation between ports.

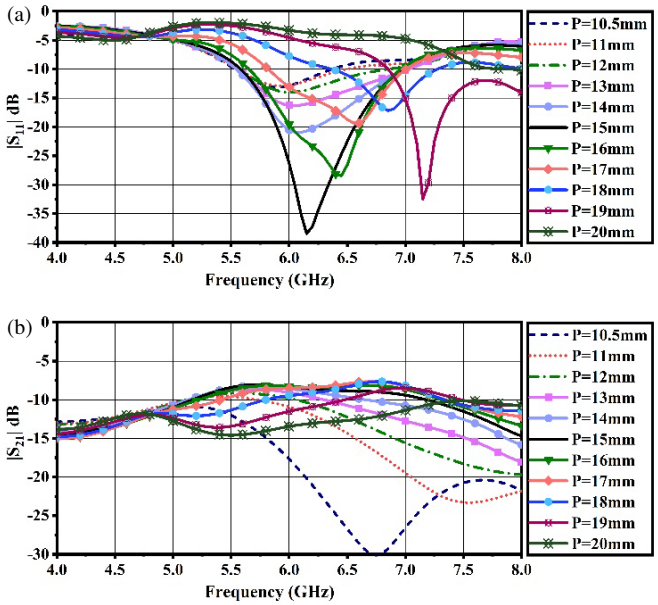

FIGURE 5. S parameter variation for different value of P. (a) Reflection coefficient. (b) Isolation between ports.

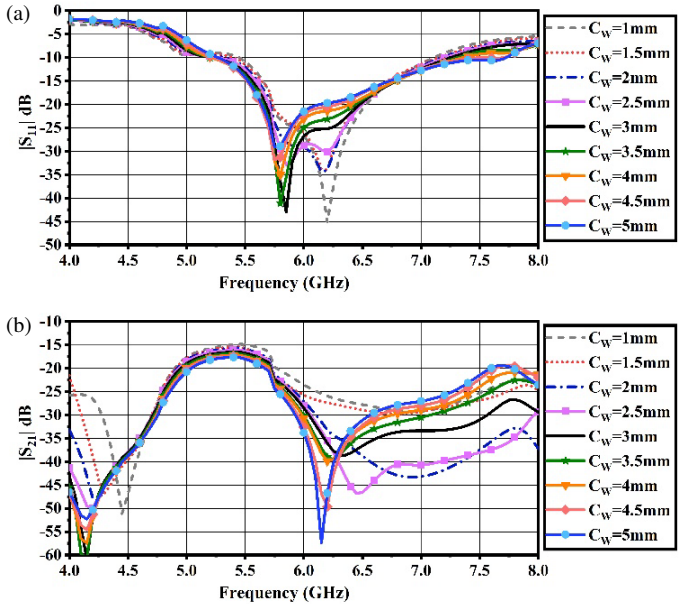

FIGURE 6. S parameter variation for different value of C_W. (a) Reflection coefficient. (b) Isolation between ports.

ing inter-port interference and enhancing overall MIMO performance. As shown in Fig. 4(b), we analyzed the effect of varying the P_i from 20 mm to 25 mm. For $P_i = 22.5$ mm, the $|S_{21}|$ remains below -15 dB within the operating bandwidth, suggesting moderate isolation. Although acceptable, this isolation level can be further improved in the next optimization step by further tuning the pin position.

5. PIN POSITION OPTIMISATION

To achieve optimal performance of the 2-port MIMO DRA, the position of the metallic pin (P) was varied from 10.5 mm to 20 mm, and its impact on both reflection coefficient $|S_{11}|$ and isolation $|S_{21}|$ was analyzed. The reflection coefficient results, shown in Fig. 5(a), reveal that a pin position of $P = 15$ mm provides the deepest resonance and the widest operational bandwidth, with $|S_{11}|$ dropping below -30 dB near 6.2 GHz. For $P = 15$ mm, the $|S_{11}|$ remains below -10 dB over the frequency range of 5.4 GHz to 7.1 GHz, resulting in an impedance bandwidth of approximately 1.7 GHz. This frequency range effectively covers the C-band of the microwave spectrum, which spans from 4 GHz to 8 GHz, meaning the antenna covers approximately 42.5% of the C-band. Additionally, the mutual coupling $|S_{21}|$, as illustrated in Fig. 5(b), remains below -15 dB across most of the band, ensuring moderate isolation between the antenna ports. While the current level of isolation is acceptable, further improvement is desired to enhance MIMO system performance. Therefore, in the next optimization step, a rectangular cavity will be introduced around the antenna structure, with its inner walls coated with copper. This modification is intended to suppress surface wave coupling and edge radiation, thereby improving both isolation and impedance bandwidth within the C-band. Hence, the choice of $P = 15$ mm serves as a strong baseline for further enhancement in the overall antenna design.

6. CAVITY OPTIMISATION

During the last phase of the development, the diagonal cavity surfaces of the DRA were coated with a thin copper metallic layer to confine near fields, suppress mutual coupling, and enhance port isolation. The copper-coated surface, which is the conductive boundary, serves as an electromagnetic barrier between the resonating elements, thus it leads to an improvement in isolation by more than 10 dB and at the same time keeps a wide impedance bandwidth. The technique is in line with the isolation-enhancement method used in the recent MIMO DRA publications, where metal patterns are utilized for controlled mode confinement and coupling suppression. A parametric sweep of the cavity width (C_W) from 1 mm to 5 mm was performed while keeping the cavity length (C_L) fixed at 26 mm, which is nearly half the diagonal length of the square DRA (30 mm $\times$ 30 mm $\times$ 30 mm). The most optimal performance was achieved at $C_W = 3$ mm. As shown in Fig. 6, the reflection coefficient $|S_{11}|$ remains below -10 dB from 5.49 GHz to 6.87 GHz, resulting in an impedance bandwidth of 1.38 GHz. This marks a notable improvement over the previous pin-optimized configuration ($P = 15$ mm), which had a bandwidth of 1.12 GHz (5.58–6.70 GHz), indicating a bandwidth enhancement of approximately 23%. Furthermore, as illustrated in Fig. 6(a), isolation $|S_{21}|$ improved significantly, dropping below -40 dB near resonance compared to -30 dB previously — reflecting an isolation improvement of over 20 dB as shown in Fig. 6(b). As a result, the antenna now covers 57.5% of the C-band (4–8 GHz), compared to 28% earlier, substantially enhancing its applicability in C-band systems. In the next step of the design process, we will optimize the cavity length while

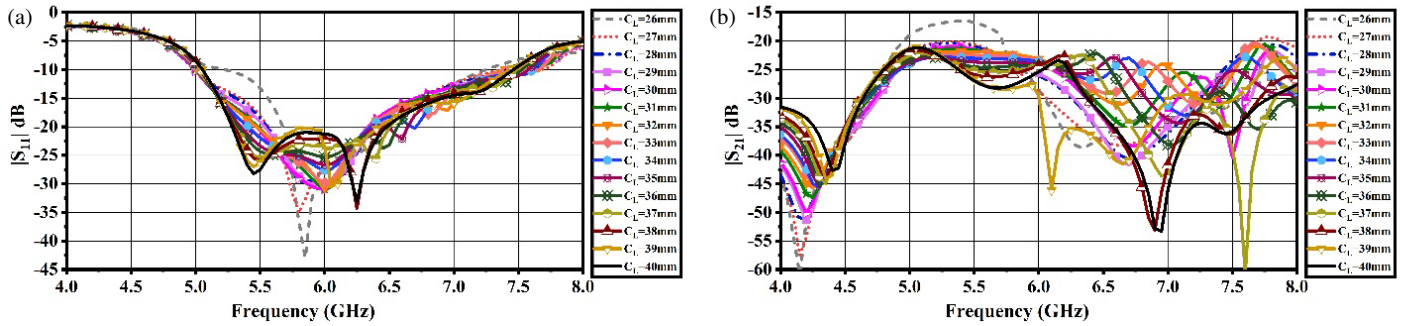

FIGURE 7. S parameter variation for different value of C_L. (a) Reflection coefficient. (b) Isolation between ports.

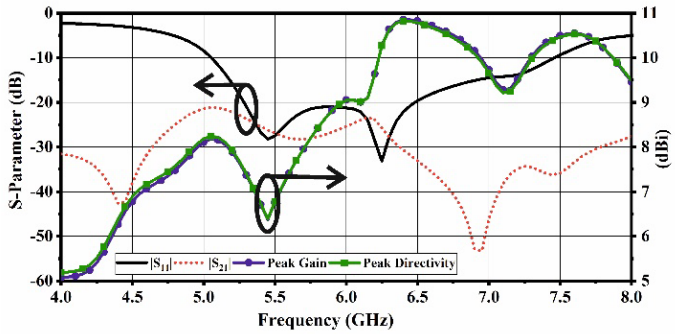

FIGURE 8. S-parameter of proposed 2-port MIMO antenna.

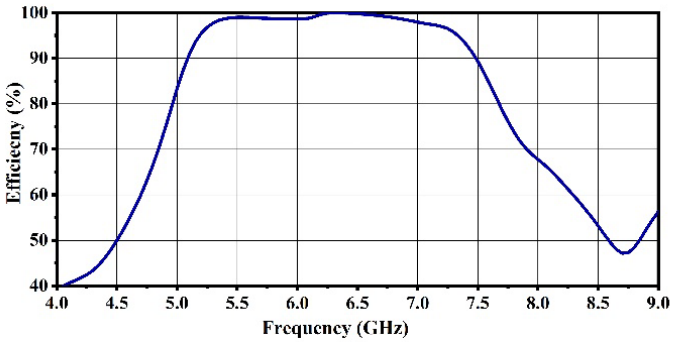

FIGURE 9. Simulated efficiency of proposed 2-port MIMO antenna.

keeping the cavity width fixed at 3 mm, with the objective of further improving both impedance bandwidth and port isolation.

In the final optimization step, the cavity length (C_L) varied from 26 mm to 40 mm while maintaining a fixed C_W of 3 mm, with the goal of further improving the antenna's impedance bandwidth and isolation. As illustrated in the $|S_{11}|$ response in Fig. 7(a), the best performance was observed for $C_L = 40$ mm, where the antenna achieved a wide impedance bandwidth ranging from 5.16 GHz to 7.26 GHz ($|S_{11}| < -10$ dB), resulting in a bandwidth of 2.10 GHz. This corresponds to approximately 70% coverage of the C-band (4–8 GHz), indicating a substantial improvement over the previous step.

The increased physical length of the resonant cavity allows it to support more closely spaced modes, enhancing energy storage, coupling in the dielectric resonator, and bandwidth. By improving the interaction between the electromagnetic field and the dielectric material, the longer cavity length effectively reduces the Q-factor and increases the bandwidth. Additionally, the cavity aids in field confinement and surface current control, which results in more effective radiation and lower return loss across a larger frequency range.

As observed in the $|S_{21}|$ response shown in Fig. 7(b), the mutual coupling (isolation) between the antenna ports was significantly improved. For $C_L = 40$ mm, the isolation remained below -30 dB throughout the operating band, with deep nulls approaching -45 dB, indicating reduced electromagnetic interference between the ports. Compared to the previous step (Fig. 6(a) and Fig. 6(b)), where only the C_W was optimized, this step achieved not only a broader impedance bandwidth but also a flatter and more stable isolation profile. These improvements further demonstrate that optimizing cavity dimensions plays a crucial role in achieving high isolation and ultra-wideband performance, making the antenna highly suitable for advanced C-band MIMO applications.

7. PROPOSED 2 PORT MIMO ANTENNA

After a thorough optimization of design parameters, including P_i, P, C_W, and C_L, the final simulated results of the proposed 2-port MIMO DRA system demonstrate excellent electromagnetic performance. As shown in Fig. 8, the reflection coefficient $|S_{11}|$ remains well below -10 dB across a wide frequency range of approximately 5.1 to 7.4 GHz corresponding to a fractional bandwidth of approximately 36.8%, indicating efficient impedance matching and low return loss. The isolation $|S_{21}|$ stays significantly below -20 dB throughout the band, confirming minimal mutual coupling between the ports, which is an essential requirement for robust MIMO operation.

Figure 8 illustrates that the peak gain reaches close to 10 dBi, while the peak directivity also aligns closely, indicating effective radiation and strong directionality with minimal losses. The increase in gain of the proposed DRA configuration is mainly due to the combined effects of the optimized dielectric resonator size and shape, the metal cavity confinement, and the accurate positioning of the excitation port. The cavity enhances the confinement of the field, thus lessening the surface wave and leakage losses and, therefore, increasing efficiency. At the same time, the best pin insertion and location allow for the strongest excitation of the fundamental resonant mode, thus,

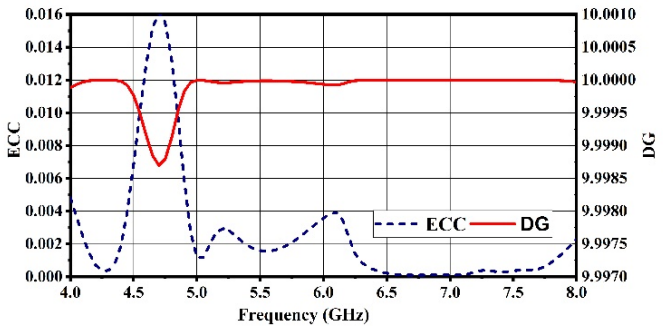

FIGURE 10. ECC and DG of proposed 2-port MIMO antenna.

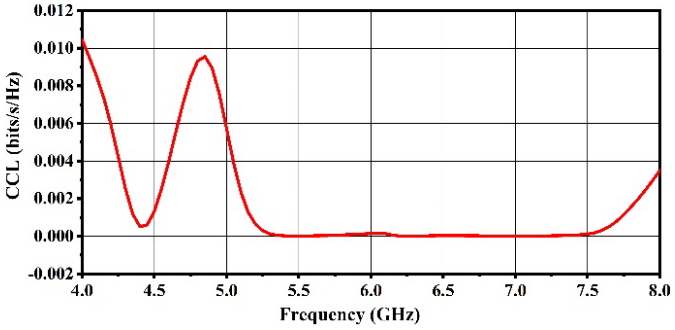

FIGURE 11. Simulated CCL of proposed 2-port MIMO antenna.

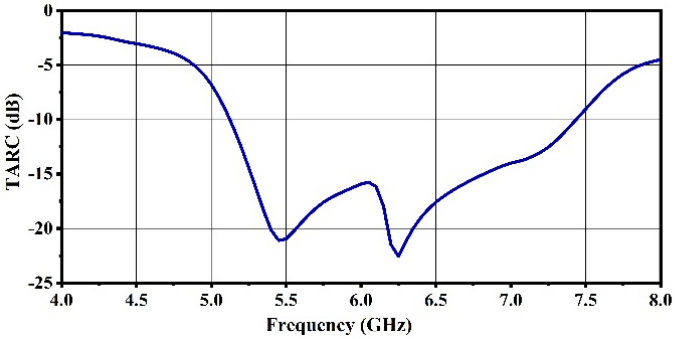

FIGURE 12. Simulated TARC of proposed 2-port MIMO antenna.

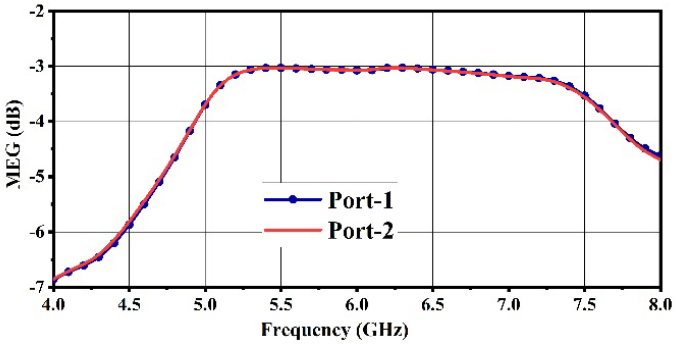

FIGURE 13. Simulated MEG of proposed 2-port MIMO antenna.

the maximum radiated field strength. In relation to this, the simulated efficiency that is illustrated in Fig. 9 is a great confirmation of the antenna's high efficiency over the whole operating bandwidth, which is the direct reason for the gain performance that has been observed.

From a diverse perspective, the antenna performs remarkably well. It can be seen in Fig. 10 that the Envelope Correlation Coefficient (ρ) remains very low, with maximum values under 0.016, and drops below 0.005 across most of the band, demonstrating excellent spatial diversity. Consequently, in Fig. 10, the Diversity Gain (G_{app}) remains close to the ideal value of 10 dB, confirming that the system can efficiently support multiple-input multiple-output (MIMO) operation without significant signal correlation or degradation.

In order to properly measure the diversity and correlation features of the suggested MIMO RDRA, three parameters, namely Channel Capacity Loss (CCL), Total Active Reflection Coefficient (TARC), and Mean Effective Gain (MEG), were evaluated based on the simulated S-parameters.

CCL measures the reduction of data capacity that can be attributed to the correlation of antenna elements and, therefore, can be represented as:

$$CCL = -\log_2(1 - ECC^2)$$

where ECC stands for the Envelope Correlation Coefficient.

To perform MIMO efficiently, the CCL value must be less than 0.4 bits/s/Hz. The CCL of the proposed MIMO stays below 0.01 bits/s/Hz in the operating bandwidth as demonstrated in Fig. 11, which is in line with the minimal correlation and high channel efficiency.

TARC evaluates the overall reflection behaviour of the multiport system when both ports are simultaneously excited. It is defined as:

$$TARC = \sqrt{\frac{|S_{11}| + |S_{12}|^2 + |S_{21}| + |S_{22}|^2}{2}}$$

A lower TARC value indicates improved impedance matching and balanced excitation. As shown in Fig. 12, the TARC of the proposed antenna remains below -10 dB throughout the band, demonstrating stable port matching and minimal power imbalance.

MEG reflects the power received by each antenna element in a multipath environment and is calculated as:

$$\text{MEG}_1(f) = 0.5 \times [1 - |S_{11}|^2 - |S_{21}|^2]$$
$$\text{MEG}_2(f) = 0.5 \times [1 - |S_{22}|^2 - |S_{12}|^2]$$

The factor 0.5 assumes equal incident power from all directions, and the expression neglects radiation efficiency since the simulated efficiency exceeds 90%. As illustrated in Fig. 13, the MEG for both ports lies between -3 dB and -4 dB, indicating balanced reception capability and effective diversity performance.

Collectively, the low CCL, low TARC, and balanced MEG values confirm that the proposed MIMO RDRA exhibits excellent isolation, impedance matching, and diversity characteristics, making it highly suitable for wideband C-band wireless communication systems.

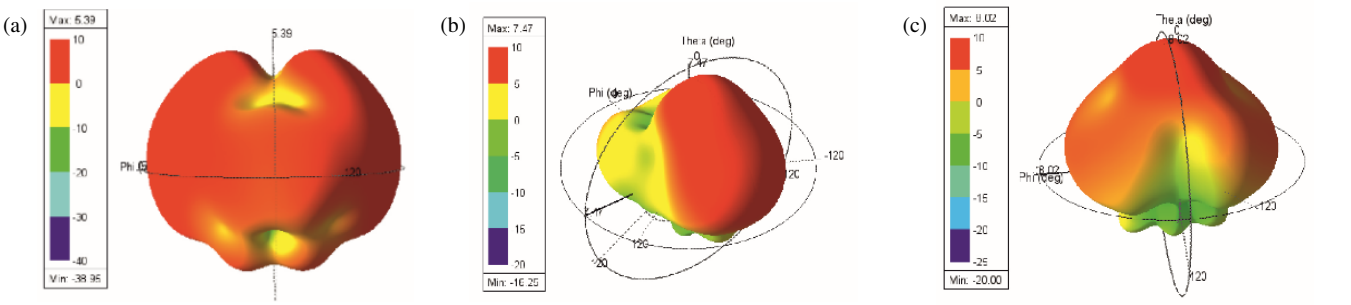

(a) Port 1-0°, Port 2-0°

(b) Port 1-0°, Port 2-90°

(c) Port 1-0°, Port 2-180°

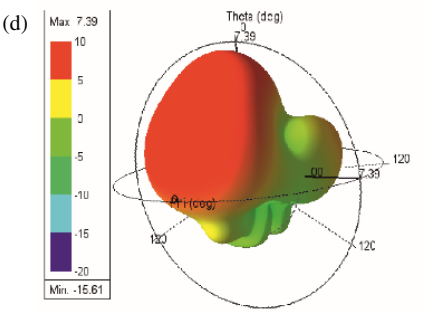

(d) Port 1-0°, Port 2-270°

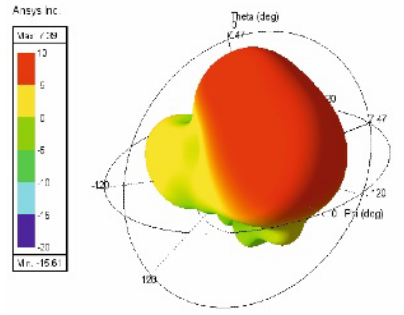

(e) Port 1-90°, Port 2-0°

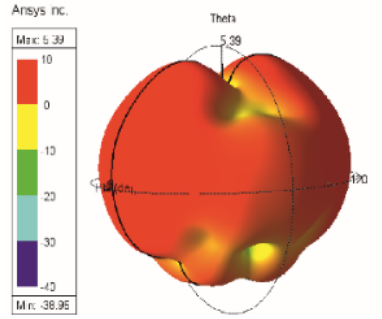

(f) Port 1-90°, Port 2-90°

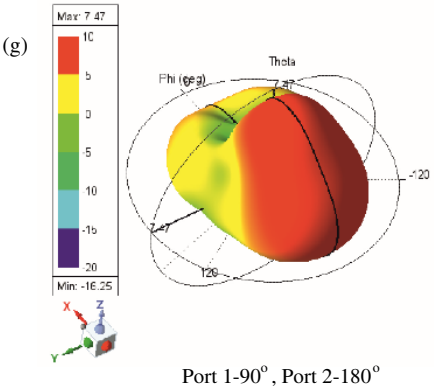

(g) Port 1-90°, Port 2-180°

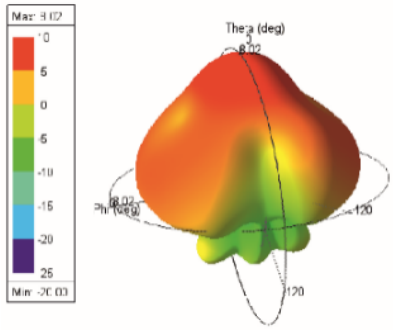

(h) Port 1-90°, Port 2-270°

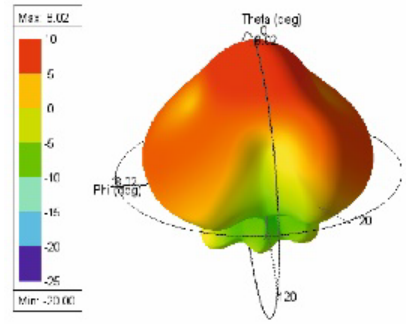

(i) Port 1-180°, Port 2-90°

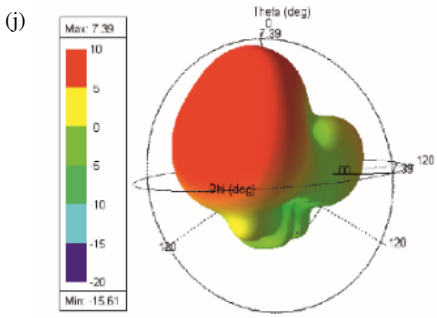

(j) Port 1-180°, Port 2-90°

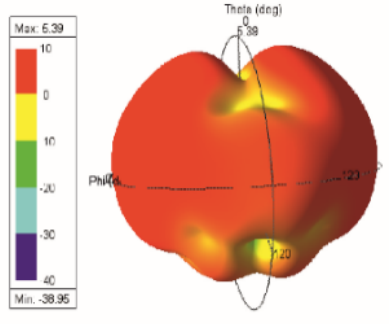

(k) Port 1-180°, Port 2-180°

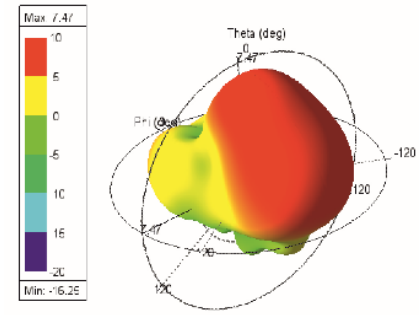

(l) Port 1-180°, Port 2-270°

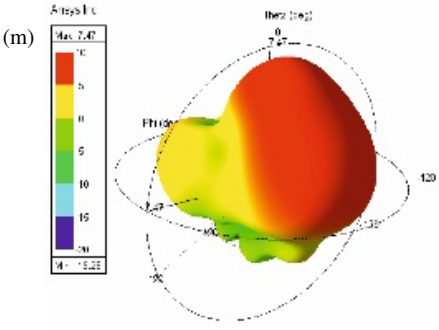

(m) Port 1-270°, Port 2-0°

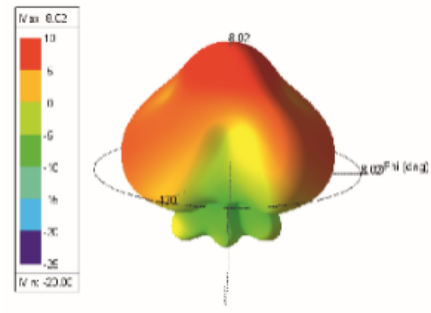

(n) Port 1-270°, Port 2-90°

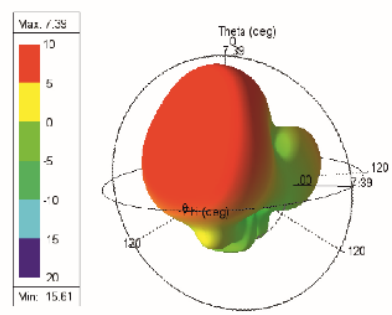

(o) Port 1-270°, Port 2-180°

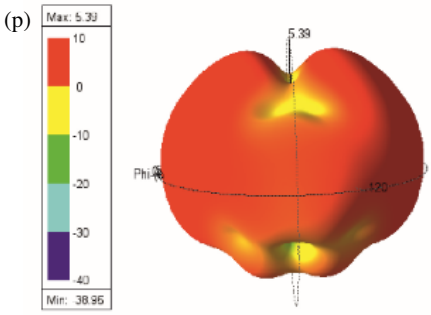

Port 1-270°, Port 2-270°

FIGURE 14. Radiation patterns under varying port phase excitations at 5.4 GHz.

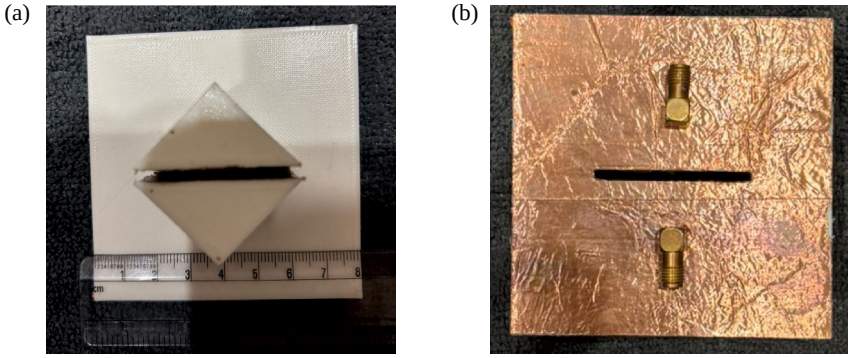

FIGURE 15. Fabricated model of proposed antenna: (a) Top view, (b) Back view.

8. RADIATION PATTERN STEERING ANALYSIS

A key functional feature of the new system is the electronic beam steering, where the phases of the two ports are adjusted to change the excitation. Different phase combinations, e.g., 0°, 90°, 180°, and 270° at 5.4 GHz (Fig. 14 and Table 1) make it possible to main beam be continuously moved over several spatial directions by phase control only, instead of changing the pattern modes. As an example, 0° phase difference results in a symmetric quasi-broadside radiation, whereas one of the quadrature phase shifts, i.e., 90° and 270°, respectively, drives the beam unidirectionally, i.e., Oblique (tilted) radiation pattern in $\pm Xm$ and 180° phase difference results in an end-fire radiation pattern in $\pm Z$ directions, and the reason is the interference of the radiated fields from both ports in the dielectric cavity. Here, the areas of the cavity, where the fields are in phase and hence combine to give a stronger field, cause enhanced radiation in the direction, while those where the fields are out of phase are responsible for the suppressed radiation in the specific directions.

Such electronic beam control, achieved without mechanical tuning or external switches, leverages mutual coupling and hybrid mode excitation within the dielectric resonators. It offers a compact and energy-efficient solution for adaptive beamforming, directional signal coverage, and interference avoidance, which are critical for modern communication systems.

Given its wide impedance bandwidth, high gain, excellent isolation, and robust diversity metrics, this MIMO DRA system operating in the C-band is highly suitable for a variety of modern wireless applications, such as:

- 5G mid-band communications (especially 3.5–6.5 GHz).
- Radar systems for weather monitoring and defense.
- Satellite communications (e.g., fixed satellite services).
- Wi-Fi 6E and Wi-Fi 7 technologies.
- Smart IoT infrastructure and vehicular communications in intelligent transport systems (ITS).

In summary, the proposed antenna system provides a compact, high-performance solution for next-generation wireless systems requiring broadband operation, high reliability, and enhanced capacity.

9. SIMULATED AND MEASURED RESULTS

As shown in Fig. 15, a prototype of the 2-port MIMO DRA was fabricated using biodegradable PLA filament and subsequently tested in a typical measurement setup. Simulated and measured S-parameters are compared. These results are depicted in Fig. 16, where the measured $|S_{11}|$ for fabricated prototype stays below -10 dB in the range of 5.05–7.3 GHz, confirming wideband impedance matching. Besides, the measured isolation $|S_{21}|$ that is still below -20 dB throughout the whole frequency band allows one to conclude that the ports are well

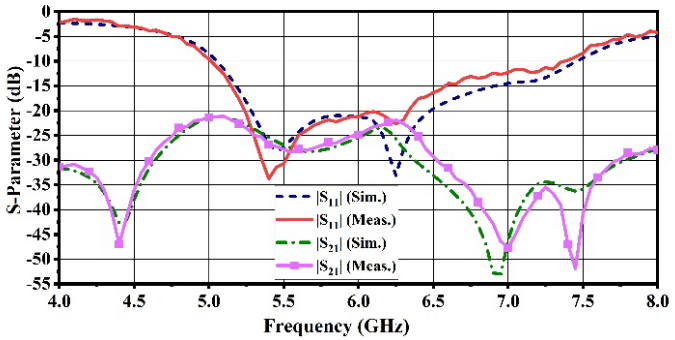

FIGURE 16. Simulated and measured S-parameters of proposed 2-port MIMO antenna.

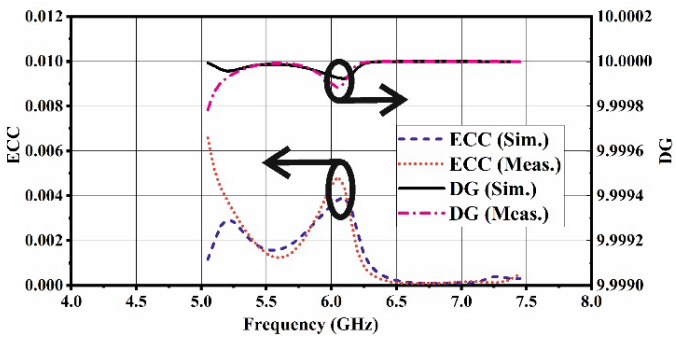

FIGURE 17. Comparison of simulated and measured correlation coefficient and diversity gain of proposed 2-port MIMO antenna.

TABLE 1. Radiation patterns under varying port phase excitations at 5.4 GHz.

Phase		Beam Type	Beam Width	Peak Gain	Beam Direction
Port-1	Port-2				
0°	0°	Quasi-Broadside	95.1	5.38	$(\pm X)$
0°	90°	Oblique	88.05	7.47	$(-X)$
0°	180°	Endfire	40.5	8.02	$(+Z)$
0°	270°	Oblique	88.86	7.39	$(+X)$
90°	0°	Oblique	88.86	7.39	$(+X)$
90°	90°	Quasi-Broadside	95.09	5.38	$(\pm X)$
90°	180°	Oblique	88.05	7.47	$(-X)$
90°	270°	Endfire	40.5	8.02	$(+Z)$
180°	0°	Endfire	40.5	8.02	$(+Z)$
180°	90°	Oblique	88.86	7.39	$(+X)$
180°	180°	Quasi-Broadside	95.09	5.38	$(\pm X)$
180°	270°	Endfire	88.05	7.47	$(-X)$
270°	0°	Oblique	88.05	7.47	$(-X)$
270°	90°	Endfire	40.5	8.02	$(+Z)$
270°	180°	Oblique	88.86	7.39	$(+X)$
270°	270°	Quasi-Broadside	95.09	5.38	$(\pm X)$

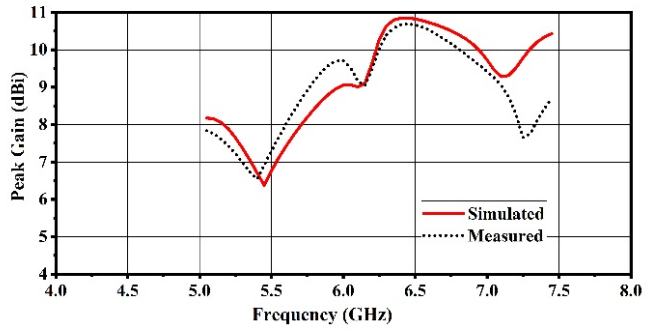

FIGURE 18. Comparison of simulated and measured peak gains of the proposed 2-port MIMO antenna.

decoupled, which is a key requirement in high-quality MIMO systems.

Figure 17 compares correlation and diversity performance. For both simulated and measured cases, the ρ is below 0.015, and G_{app} approaches the ideal 10 dB value. These results support low mutual correlation and strong MIMO diversity.

Simulated and measured peak gain values are depicted in Fig. 18, where a strong agreement between the two sets of data can be seen. Above 10 dBi gain is obtained in the higher frequency region. Some changes can be observed that could be due to the 3D printing process and material dielectric losses of the PLA filament.

For the purpose of radiation characterization, Fig. 19 illustrates the normalized 2D radiation patterns in the XZ-plane at 5.4 GHz for different phase combinations between Port 1 and Port 2. Given that simulation and experiment agree in result, it can be concluded that the beam remains steerable. When in-phase excitation is applied, for example, 0°–0°, 180°–180°, the radiation pattern is mainly directed in the broadside direction, while out-of-phase and quadrature combinations of 0°–90°, 90°–180° produce tilted beams in various directions. The possibility to regulate the beam direction efficiently by port phase shifts thus becomes a radiation pattern steerable feature,

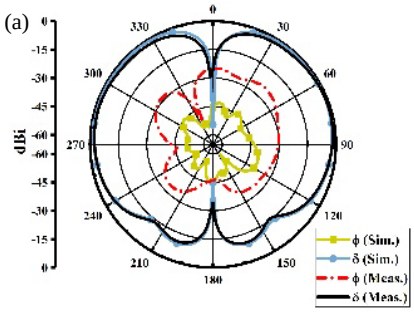

Port 1-0°, Port 2-0°

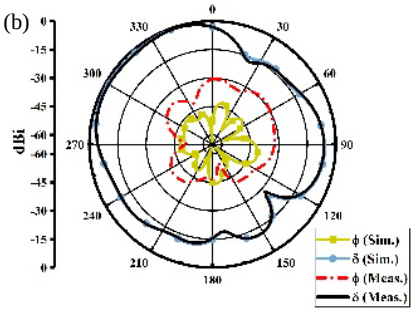

Port 1-0°, Port 2-90°

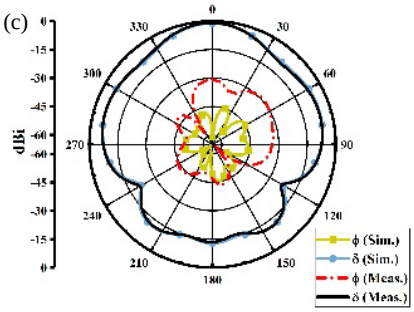

Port 1-0°, Port 2-180°

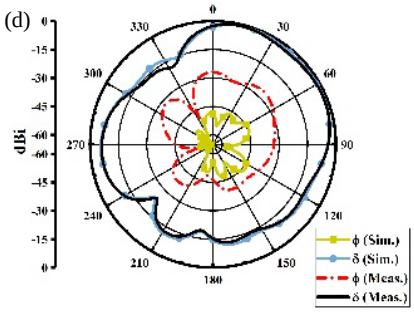

Port 1-0°, Port 2-270°

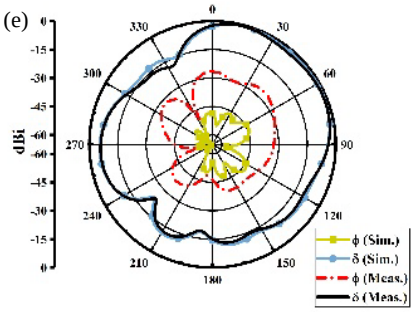

Port 1-90°, Port 2-0°

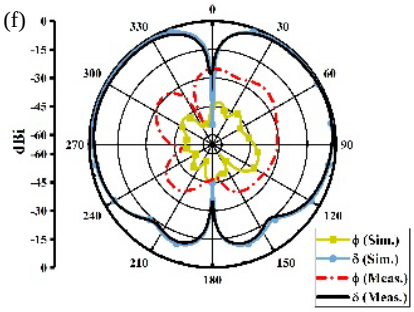

Port 1-90°, Port 2-90°

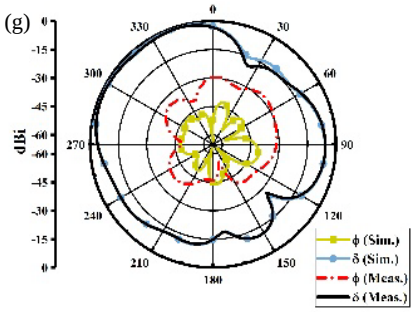

Port 1-90°, Port 2-180°

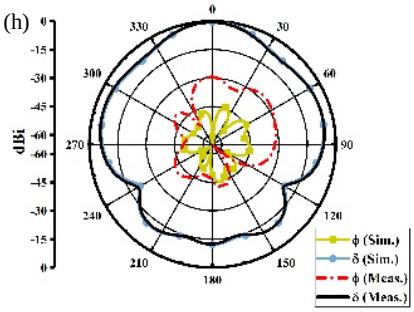

Port 1-90°, Port 2-270°

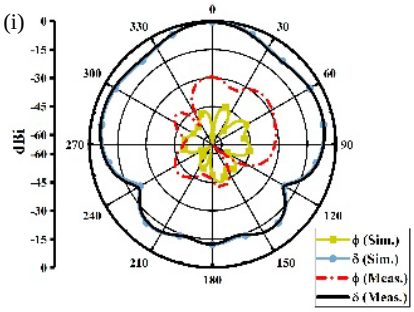

Port 1-180°, Port 2-0°

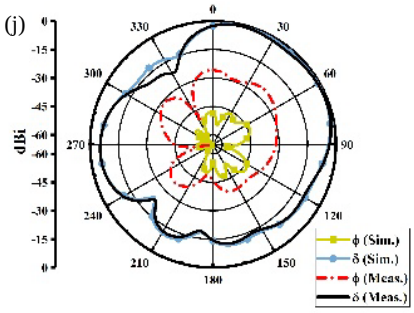

Port 1-180°, Port 2-90°

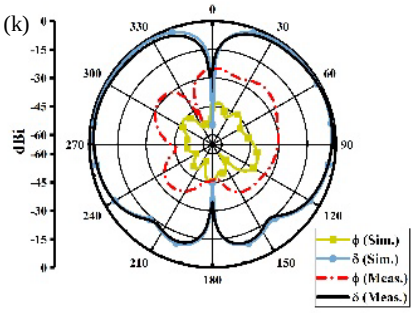

Port 1-180°, Port 2-180°

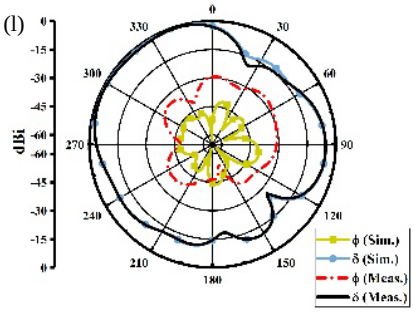

Port 1-180°, Port 2-270°

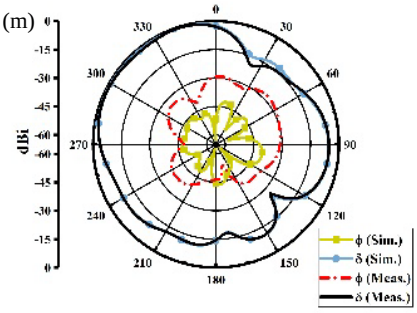

Port 1-270°, Port 2-0°

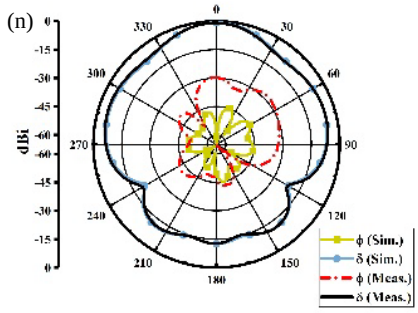

Port 1-270°, Port 2-90°

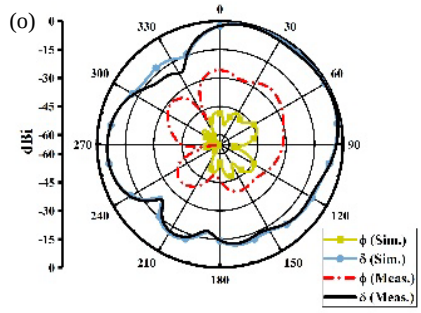

Port 1-270°, Port 2-180°

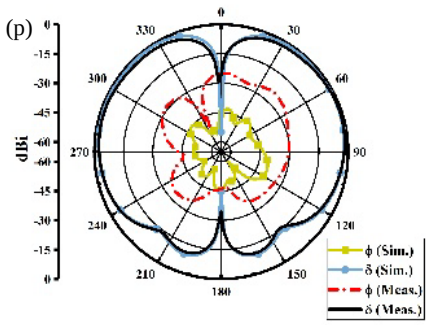

Port 1-270°, Port 2-270°

FIGURE 19. Simulated and measured normalized radiation patterns at 5.4 GHz for different port phase configurations.

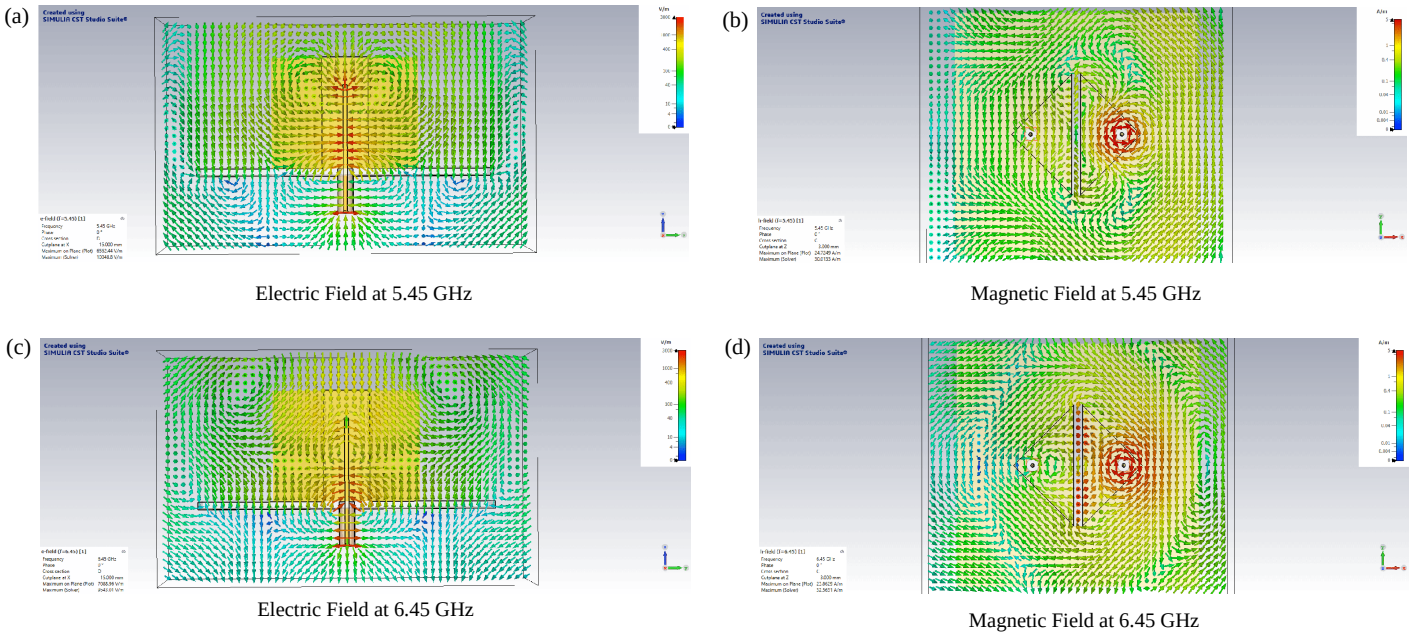

Electric Field at 5.45 GHz

Magnetic Field at 5.45 GHz

Electric Field at 6.45 GHz

Magnetic Field at 6.45 GHz

FIGURE 20. Simulated field distributions of the proposed MIMO DRA at 5.45 GHz and 6.45 GHz, illustrating the excited hybrid mode.

so the proposed design is very relevant for adaptive beamforming, directional communication, and interference mitigation in C-band applications. rent port phase configuration.

A thorough modal analysis was carried out to grasp the wideband operation of the proposed dielectric resonator antenna by looking at electric and magnetic field distributions at two resonances that correspond to the lower and upper edges of the band of the operation. The fundamental $\mathrm{HEM}_{11}\delta$ mode features can be recognized from the image of the first resonant mode, Fig. 20(a). Around 5.45 GHz, the E-field lines are mainly along the vertical axis of the DRA, and the circular loops can be seen in the center of the H-field that is the magnetic field of the fundamental $\mathrm{HEM}_{11}\delta$ mode in Fig. 20(b). On the other hand, at the upper resonance close to 6.45 GHz, the E-field patterns in Fig. 20(c) have changes regarding complexity, as they have an additional null/phase reversal region and a larger circulation of the H-field in Fig. 20(d). These properties point to the generation of a high-order hybrid mode like $\mathrm{HEM}_{12}\delta$ or TE_{121}, which contains the additional resonant energy.

By the precise manipulation of the cavity shape and excitation pin height, the two modal resonances are made near each other so that the modal transition is smooth, and the impedance response is effectively merged, which produces wideband performance as measured. The modal merging demonstrated here is in line with the modal merging mechanism recently reported for wideband DRAs, e.g., those in [4].

A detailed comparison of the proposed MIMO RDRA with the recently published C-band DRA is given in Table 2. It shows that the antenna made of biodegradable PLA has the widest bandwidth ($\sim$ 35%) among all works compared, and at the same time it keeps high port isolation ($>$ 20 dB) and excellent diversity characteristics (ECC $<$ 0.015). The antenna is also capable of delivering a peak gain of more than 10 dBi, which is quite competitive with few ceramic-based designs in spite of the lower permittivity of PLA. Electrically, the proposed structure corresponds to the dimensions of $0.625\lambda \times 0.625\lambda \times 0.625\lambda$, which is quite small for the dielectric constant of the material.

TABLE 2. Performance comparison between the proposed PLA-based 3D-printed MIMO rectangular dielectric resonator antenna and previously published state-of-the-art C-band DRA designs.

Reference & Material	Bandwidth (GHz)	% B.W.	Peak Gain (dBi)	Isolation (dB)	ECC	Size (mm^3)	Electrical Size (λ_0)	Pattern Reconfigurable	Notable Contributions
[P.D., PLA, 3D-printed]	5.1–7.4	$\sim 35\%$	> 10	> 20	< 0.015	$30 \times 30 \times 30$	$0.625\lambda \times 0.625\lambda \times 0.625\lambda$	Yes (beam steering)	Wideband, bio-based, high isolation
[Ref. [1]] [Ceramic]	5.7–6.7	$\sim 17\%$	8.5	17	0.02	$32 \times 30 \times 28$	$0.64\lambda \times 0.60\lambda \times 0.58\lambda$	No	Conventional DRA
[Ref. [2]] [Ceramic]	5.2–6.2	$\sim 17\%$	9	18	0.02	$33 \times 30 \times 30$	$0.66\lambda \times 0.62\lambda \times 0.62\lambda$	No	Wideband, no reconfigurability
[Ref. [3]] [Ceramic, 3D-print]	5.5–7.0	$\sim 24\%$	9.5	20	0.018	$30 \times 30 \times 31$	$0.62\lambda \times 0.62\lambda \times 0.64\lambda$	No	3D-printed, conventional
[Ref. [4]] [High-ε_r Ceramic]	3.3–3.8	$\sim 14\%$	11–12	> 18	< 0.02	$28 \times 28 \times 35$	$0.33\lambda \times 0.33\lambda \times 0.41\lambda$	No	Dual-pol, high-gain, compact ceramic DRA

P.D. — Proposed Design

As a result of comparison with high-permittivity ceramic antennas (Refs. [1–4]) including the newly published design by El Yousfi et al. [4], which attains a smaller electrical footprint because of its high ε_r, the proposed antenna still offers extra functional features. To be exact, the current invention can switch its radiation pattern (beam steering), besides which the ceramic DRAs listed in Table 2 cannot. Moreover, by using 3D-printed PLA, the following benefits can be achieved: low fabrication cost, easy prototyping, eco-friendliness, and the capability to complex internal geometries that are hard to manufacture with a brittle ceramic. The performance and fabrication benefits taken together make the proposed design highly compatible with modern wideband and high-isolation C-band MIMO communication systems.

10. CONCLUSION

This paper has reported a two-port MIMO dielectric resonator antenna (DRA) system made from environmentally friendly polylactic acid (PLA) using the additive manufacturing technique. The antenna design was extensively explored by adjusting the parameters, such as the pin height, pin position, cavity width, and cavity length in order to get very good electromagnetic performance in the C-band.

The developed prototype demonstrated a broad simulated impedance bandwidth ranging 5.1 to 7.4 GHz corresponding to a fractional bandwidth of approximately 36.8%, within which the return loss ($|S_{11}|$) remained below -10 dB, and the isolation ($|S_{21}|$) exceeded -20 dB, indicating minimal mutual coupling and effective port decoupling. Both simulated and experimental results revealed a peak gain greater than 10 dBi, a low envelope correlation coefficient (ECC < 0.015), and an almost ideal diversity gain (DG ≈ 10 dB), thereby substantiating the antenna's suitability for integration into MIMO systems.

One amazing point in this scientific research work is the demonstration of the electronic beam steering — the capability of guiding the main lobe direction by changing the phase difference between the excitation ports. The mentioned 2D radiation patterns demonstrate that the main beam is turned dynamically in the XZ-plane by phase control, thus allowing spatial selectivity and adjustable coverage for next-generation wireless systems. This method merely allows for gradual and continuous directional change rather than switching from radically different radiation patterns.

Based on the broadband capability, high isolation, strong gain, low ECC, and beam steering capability of the proposed MIMO DRA system, it is ideal for various C-band applications such as 5G base stations, satellite downlink services, radar systems, Wi-Fi 6E/7, and smart vehicular or IoT communications. The adoption of sustainable PLA material and 3D printing not only allows for environmentally friendly and cost-efficient antenna manufacturing but also facilitates the rapid prototyping of innovative wireless technologies.

REFERENCES

[1] Ahmad, H., M. H. Jamaluddin, F. C. Seman, and M. Rahman, "MIMO dielectric resonator antennas for 5G applications: A review," *Electronics*, Vol. 12, No. 16, 3469, 2023.

[2] Harkare, A. H., A. G. Kothari, A. A. Bhurane, M. P. Abegaonkar, and P. Patel, "A compact dielectric resonator antenna with wideband circular polarization characteristics for C and X-band applications," *Microwave and Optical Technology Letters*, Vol. 66, No. 7, e34241, 2024.

[3] Ahmad, H., M. H. Jamaluddin, F. C. Seman, M. Rahman, N. Nasir, and A. Ayub, "Compact dual-band enhanced band-

width 5G mm-wave MIMO dielectric resonator antenna utilizing metallic strips," *AEU — International Journal of Electronics and Communications*, Vol. 187, 155510, 2024.

[4] El Yousfi, A., K. A. Abdalmalak, A. Lamkaddem, A. M. Barrera, B. Biscontini, and D. Segovia-Vargas, "Miniaturized dual-polarized, high-gain, and wideband dielectric resonator antenna for low band massive MIMO applications," *Progress In Electromagnetics Research*, Vol. 179, 101–111, 2024.

[5] Muttair, K. S., O. A. Shareef, and H. B. Taher, "Designs, developments, challenges, and fabrication materials for MIMO antennas with various 5G and 6G applications: A review," *International Journal of Microwave and Wireless Technologies*, Vol. 16, No. 9, 1510–1539, 2024.

[6] Merlos-Garza, E., Z. U. Khan, and S. K. Khamas, "A compact MIMO rectangular dielectric resonator antenna for millimeter-wave communication," *Electronics*, Vol. 13, No. 16, 3280, 2024.

[7] Dhananjeyan, R., S. Ramesh, D. R. Kumar, and O. P. Kumar, "Compact octagonal MIMO antenna system for broadband applications with enhanced isolation and wideband performance," *Scientific Reports*, Vol. 15, No. 1, 18921, 2025.

[8] Sharma, P., R. N. Tiwari, P. Singh, P. Kumar, and B. K. Kanaujia, "MIMO antennas: Design approaches, techniques and applications," *Sensors*, Vol. 22, No. 20, 7813, 2022.

[9] Votis, C., G. Tatsis, and P. Kostarakis, "Envelope correlation parameter measurements in a MIMO antenna array configuration," *International Journal of Communications, Network and System Sciences*, Vol. 3, No. 4, 350–354, 2010.

[10] El Hadri, D., A. Zugari, A. Zakriti, and M. E. Ouahabi, "Dual-band MIMO antenna with four CPW elements using polarization diversity for 5G mobile communication networks and satellite," *Advanced Electromagnetics*, Vol. 12, No. 3, 43–53, 2023.

[11] Yurduseven, O., S. Ye, T. Fromenteze, B. J. Wiley, and D. R. Smith, "3D conductive polymer printed metasurface antenna for Fresnel focusing," *Designs*, Vol. 3, No. 3, 46, 2019.

[12] Aydın, E. A., M. B. Biçer, M. E. Mert, C. Özgür, and B. D. Mert, "3D-printed antenna design using graphene filament and copper tape for high-tech air components," *SAE International Journal of Aerospace*, Vol. 16, No. 2, 131–140, 2023.

[13] Stopforth, R., "Conductive polylactic acid filaments for 3D printed sensors: Experimental electrical and thermal characterization," *Scientific African*, Vol. 14, e01040, 2021.

[14] Zhang, J., S. Dong, D. M. Alsekait, I. Khan, P.-C. Wang, and I. A. Hameed, "Design and performance optimization of a novel lens antenna for emerging beyond 5G wireless applications," *Frontiers in Materials*, Vol. 11, 1479398, 2024.

[15] Shang, Y., Q. Zeng, W. Cui, X. Wang, and G. Zheng, "Design of pattern reconfigurable patch antenna array based on reflective phase-shifter," *International Journal of Antennas and Propagation*, Vol. 2022, No. 1, 2803285, 2022.

[16] Zhou, Z., J. Ding, and R. Zhang, "Polarforming design with phase shifter based polarization reconfigurable antennas," *ArXiv Preprint ArXiv:2505.21990*, 2025.